

## Single-mode unidirectional microcavity laser

ZHEN-NAN TIAN,<sup>1</sup> FENG YU,<sup>1</sup> YAN-HAO YU,<sup>1</sup> JUN-JIE XU,<sup>1</sup> QI-DAI CHEN,<sup>1,\*</sup> AND HONG-BO SUN<sup>1,2</sup>

<sup>1</sup>State Key Laboratory on Integrated Optoelectronics, College of Electronic Science and Engineering, Jilin University, Changchun 130012, China

<sup>2</sup>College of Physics, Jilin University, Changchun 130012, China

\*Corresponding author: chenqd@jlu.edu.cn

Received 7 February 2017; revised 14 March 2017; accepted 14 March 2017; posted 17 March 2017 (Doc. ID 286216); published 11 April 2017

**In this Letter, we report a suspended whispering gallery mode microdisk with a hole pierced through its surface. The novel disk is made up of Rhodamine *B*-doped resin, which is fabricated by femtosecond laser direct writing technology. The pierced microcavity achieves highly directional emission of single-mode lasing with a far field divergence angle of about 10 deg, and its high *Q* factor exceeds  $2.6 \times 10^3$ . The excellent properties are confirmed by numerical simulation based on the finite-difference time-domain method. The effect of the pierced hole on the microcavity performance is discussed in detail. The method is easy to implement and has a guiding significance for improving the characteristics of an existing microcavity by simple modification.** © 2017 Optical Society of America

**OCIS codes:** (140.3945) Microcavities; (230.3990) Micro-optical devices; (220.4000) Microstructure fabrication.

<https://doi.org/10.1364/OL.42.001572>

Because of the total internal reflection of light at the periphery of a rotational symmetrical cavity, light is strongly confined in dielectric microcavities to produce discrete resonant modes, which are usually called whispering gallery modes (WGMs) [1–4]. WGM microcavities such as microdisk, microring, and microsphere have attracted much attention in applications of nonlinear optics [5], quantum electrodynamics [6], biosensing [7], and low threshold lasers [8] because of their high quality factor, low lasing threshold, and small mode volume in the last decades [9–12]. However, the applicability of those cavities is limited by isotropic light emission and multiple-mode lasing. Many methods have been proposed to realize unidirectional emission by breaking the rotational symmetry of a microdisk. The cavities deformed, such as annular cavity [13], pillar cavity [14] and spiral cavity [15], have achieved emitting light at a particular direction but with multiple-mode lasing. To gain single-mode lasing, J. F. Ku fabricated the coupled WGM microdisks of various sizes without good unidirectional emission [16]. The single-mode laser directional emission has attracted extensive attention of researchers.

Wiersig reported numerical results for a microdisk with a suitably positioned air hole to support high-*Q* modes with unidirectional light emission [17]. In addition, the air hole has an important effect on the light mode of the microcavity, which

can significantly reduce the number of lasing modes. However, the unidirectional emission of the microdisk with a hole has not been confirmed through the experiment. Recently, because of its unique high precision three-dimensional (3D) prototyping capability [18–23], femtosecond laser direct writing (FsLDW) has been used to fabricate microcavities in glass and polymer [24–26]. In this Letter, we experimentally accomplished the fabrication of a suspended WGM microdisk with a hole pierced through the disk surface by FsLDW via two-photon polymerization of dye-doped resin, which produces the unidirectional emission of single-mode lasing. Because of the low cost and good chemical/biocompatibility of polymer materials, polymer WGM microcavities with single-mode and unidirectional emission would be great potentially applied in organic optoelectronic integrated devices.

The pierced microdisk was fabricated by femtosecond pulse induced two-photon polymerization of Rhodamine *B*-doped commercial negative photoresist SU-8 (2025, MicroChem). Femtosecond laser pulses (pulse width of 120 fs, wavelength of 800 nm, repetition rate of 82 MHz) from a Ti:sapphire oscillator (Tsunami, Spectra-Physics) were tightly focused into the photoresist by a high numerical aperture ( $NA = 1.4$ ) oil immersion objective lens (100 $\times$ ) to induce polymerization in the focus spot area. The focus spot was scanned in the horizontal plane with a two-galvano mirror set, and along the optical axis by the piezo stage. All the 3D motion accuracies are around 1 nm. The dye used as a gain medium was added into the photoresist, which was 5-times diluted with cyclopentanone. After 24 h, the dye was fully mixed with the diluted photoresist. The concentration of dye in the original photoresist is about 1.5 wt. %, which is based on the results of a previous optimization experiment [16]. The dye-doped SU-8 was spin-coated on a cover glass that was cleaned with acetone and absolute ethanol for 20 min. Through the prebake, 30 min at 95°C, the solvent was evaporated, and a film around 20  $\mu\text{m}$  thick was formed. According to the preprogrammed fabrication pattern, the laser focus spot was scanned in the sample film point by point from the bottom slice to the upside. The average pulse power was only 7 mW, measured before objective lens toward the laser. The scanning step length was fixed at 100 nm in three dimensions, and exposure duration of each voxel was 500  $\mu\text{s}$ . After scanning, the patterned sample was post-baked on the hotplate for 15 min at 95°C. When the sample was cooled down, the cover glass was immersed in the developer for 15 min to remove

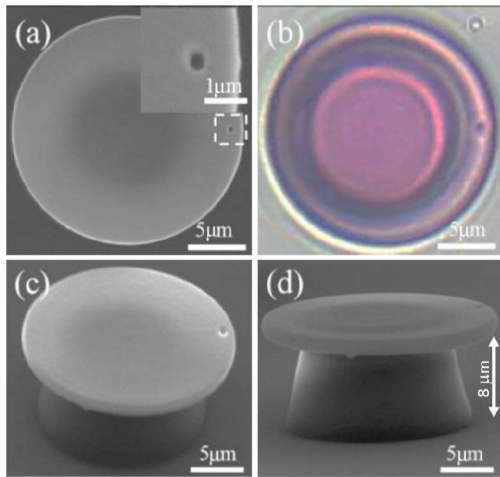


**Fig. 1.** Geometric morphology of the pierced microdisk. (a) The top view scanning electron microscopy (SEM) image. The inset shows the local amplification image of the microdisk. (b) The optical microscope photograph of the pierced microdisk. The center region with deeper color is the cone-shape pedestal shown in Fig. 1(d). (c)–(d) The 45 deg tiled view and the side view of the microdisk SEM image.

the unpolymerized photoresist, leaving a designed structure on the chip. The roughness is less than 10 nm on  $10\ \mu\text{m} \times 10\ \mu\text{m}$  planar squares [27].

The fabricated pierced microdisk was characterized by scanning electron microscopy (SEM, JSM-7500F, JEOL). Figure 1(a) shows the top view SEM image of the microdisk with a diameter of  $20\ \mu\text{m}$ , and the inset shows the amplification image of the marked area, which gives the hole size of  $0.6\ \mu\text{m}$ . The center of the small hole is only  $1\ \mu\text{m}$  from the edge of the microdisk. Shown in Fig. 1(b) is the optical microscope image of the microdisk. The microdisk color is pink, which shows that the dye is uniformly doped into the disk. Light is confined within a microcavity based on total reflection at the edge of the microcavity, which is closely related to the refractive index difference between the microcavity and its surrounding medium. To obtain a more strongly confined light property, the microdisk was designed to be a suspended structure with a cone-shape pedestal below. Figures 1(c) and 1(d) show the 45 deg tiled view and the side view of the microdisk SEM image, respectively. The vertical distance is about  $8\ \mu\text{m}$  from the cover glass to the microdisk edge.

The absorption spectrum of the mixture (SU-8 and Rhodamine B) ranges from 460 nm to 590 nm, and its photoluminescence spectrum range is 580–700 nm [4]. Therefore, a 532 nm (frequency doubled from a 1064 nm laser) picosecond laser (pulse width of 15 ps, repetition rate of 50 KHz) was used as the excitation source. A schematic diagram of excitation and collection system is shown in Fig. 2(b). A shutter with an opening time of 20 ms was used to avoid the bleaching effect of the dye molecules in the microdisk, which depends on the pump laser power and exposure time. The pump laser was focused onto a single microdisk by an objective lens (NA = 0.25,  $10\times$ ). To reduce the effect of pump position and prevent high pump power density from damaging the dye-doping structure, the microdisk was placed before the focal plane, where the size of pump laser spot was equal to

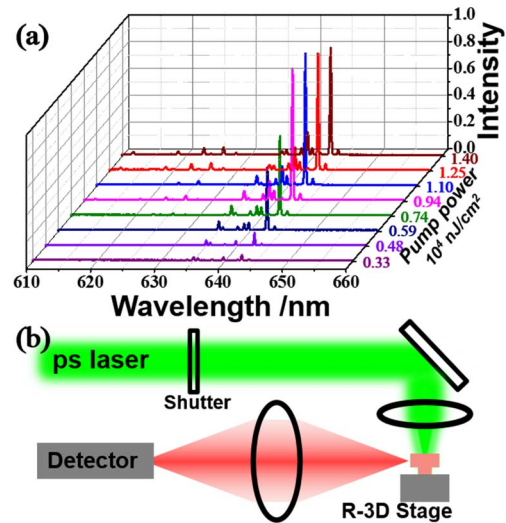


**Fig. 2.** (a) Normalized 3D-waterfall arranged emission spectrum from a  $20\text{-}\mu\text{m}$ -diameter pierced microdisk pumped with increasing power intensities of 532 nm picosecond laser. (b) The schematic diagram of excitation and collection system. The microdisk was placed on a R-3D stage composed of a rotary stage and a 3D displacement platform.

the microdisk. Lasing light was collected by a convex lens (diameter of  $25.4\ \text{mm}$ ,  $f = 30\ \text{mm}$ ) in the microcavity plane, and the spectrum was measured by a spectrometer (SR-303I-A, Andor) equipped with a charge coupled device (CCD, DV420A-OE, Andor) camera by setting the probe at the focus of the emission light. To control precisely the position and the orientation of the pierced microdisk, it was placed on a manual 3D displacement platform (accuracy of  $2\ \mu\text{m}$ ) that was fixed on a stepper motor rotary stage (accuracy of  $0.873\ \text{mrad}$ ). The emission spectra of a pierced microdisk gained with different pump power density was measured as shown in Fig. 2(a). The weak sharp peaks emerge when the power density is relatively low ( $0.33 \times 10^4\ \text{nJ}/\text{cm}^2$ ); the lasing peak appears at 642.7 nm. As the power density further increases, the lasing output increases rapidly, which can be expressed to lasing action occurring in the microcavity. The lasing wavelength does not change with the increase of pump density. Moreover, in Fig. 2(a), it can be clearly seen that the emission spectra show a single-mode lasing line while other modes are suppressed greatly compared with the multiple-mode lasing of a complete single microdisk [4].

Figure 3 shows the relationship of pump laser power and emitting light intensity at 635.1, 639.7, 642.7, and 643.9 nm. It can be found that the intensity of all emitting light was weak at a low pump laser power. The resonant process of optical amplification has not occurred. With the increase of pump intensity, the emitting light with a wavelength of 642.7 nm rises abruptly. However, other emitting light is still weak, without an obvious difference in the whole process of increasing pump power. The intensity of 642.7 nm light began to increase at about  $0.33 \times 10^4\ \text{nJ}/\text{cm}^2$ , which determines the lasing threshold. The value of the lasing threshold is smaller by an order magnitude than that reported in [15]. This is because holes are introduced into the microdisk and reduce the laser threshold by perturbing the nonlasing modes, which gives

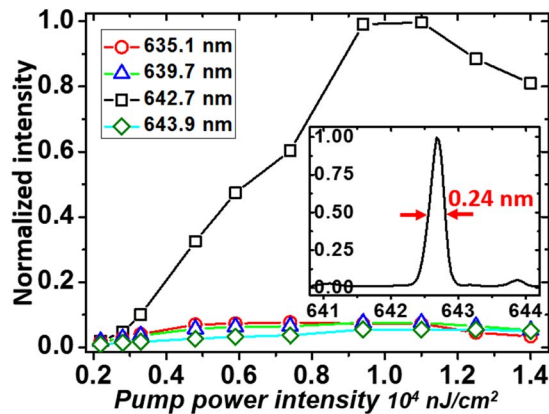


**Fig. 3.** Measured intensity of output light varies with the power of the pump laser. The light with a wavelength of 642.7 nm is amplified and shows the lasing property. However, the other light, with wavelengths of 635.1, 639.7, and 643.9 nm, cannot be amplified. The inset shows the spectrum enlargement at a wavelength of 642.7 nm with pump power intensity of  $1.1 \times 10^4$  nJ/cm<sup>2</sup>.

the lasing mode more competitive ability [28]. The lasing intensity increases linearly until the pump power reaches  $1.0 \times 10^4$  nJ/cm<sup>2</sup>, where the light output becomes saturated. The output decreases slowly with the pump power increasing continuously because of gain saturation and the photobleaching effect of the dye. The inset of Fig. 3 shows a magnitude spectrum at wavelength of 642.7 nm, whose full width at half-maximum (FWHM) is 0.24 nm. The  $Q$  factor of the microcavity can be roughly calculated according to the equation of  $Q = \lambda/\delta\lambda$ , where  $\lambda$  is the resonance wavelength and  $\delta\lambda$  is FWHM of the lasing line. Based on the measured lasing spectrum, the FWHM of the laser line at 642.7 nm was measured to be 0.24 nm, which corresponds to a  $Q$  factor of 2678. It is undeniable that the  $Q$  factor is low compared with semiconductor microcavity. However, it is still higher than polymer microcavity [29], which is widely acknowledged for its unique advantages, such as arbitrary shaping, easy integration, and low cost.

To characterize the directional emission property of the microcavity with a hole pierced, we measured the angular dependence of the emission spectrum. Experimentally, the power density of the pump laser was fixed at  $1.1 \times 10^4$  nJ/cm<sup>2</sup>. Figure 4(a) shows the lasing spectrum from five different collection angles—0, 10, 120, 240, and 300 deg—where 0 deg represents the direction on the opposite side of the small hole. From the spectra detected from specific angles, we can clearly find that the lasing intensity of the direction of 0 deg was far stronger than the intensities of other degrees. Moreover, the lasing intensities distribution with the wavelength of 642.7 nm in a polar coordinate is shown in Fig. 4(b). From the intensity distribution pattern, it is clear that the pierced microcavity has an excellent unidirectional emission property with a far field divergence angle of about 10 deg. X. P. Zhan reported that a spiral cavity exhibited a divergence angle of about 40 deg [15]. The hole is an important element for achieving unidirectional emission of single-mode lasing [28]. A systematic study on the effects of different hole parameters such as numbers, diameters, and relative positioning on the microlaser lasing will be conducted in the future.

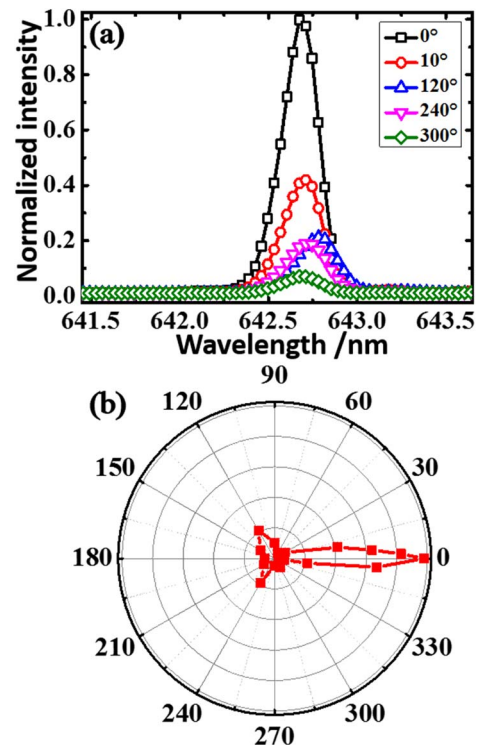


**Fig. 4.** Characterization of the directional emission property of the pierced microdisk. (a) The emission spectrum of the pierced microdisk at different detection angles. (b) The relationship of lasing intensity distribution with detection angles at a wavelength of 642.7 nm. The definition of the initial angle is the same as Fig. 5(a).

For a more detailed analysis on the contribution of the hole to the property of the microcavity laser, we carried out a two-dimensional finite-difference time-domain (FDTD) numerical simulation on a microdisk with a pierced hole (Fig. 5). The diameters of the microdisk and the hole are 20  $\mu$ m and 0.6  $\mu$ m, respectively. The minimum distance is only 400 nm from the hole to the edge of the microdisk. The length and width of the whole simulation space are 36  $\mu$ m and 31  $\mu$ m, respectively. To get closer to free space, the edge of the simulation area is set up to be a perfect matching layer with a thickness of 1  $\mu$ m. A broadband pulse of 630–650 nm is added at the edge area of the microdisk to excite all the optical modes in the cavity. With the pulse transmission in the disk, the light that cannot resonate will gradually disappear. Finally, the optical intensity distribution of the resonant light with a wavelength of 632.8 nm is shown in Fig. 5. The resonant wavelength in simulation is different from the emission laser in the experiment because the numerical simulation is based on an ideal size and device structure, which is a different situation from an experiment. Nonetheless, the optical intensity distribution in the simulation result is still very convincing. In Fig. 5(a), most of the light is confined within the microdisk and transmits along the interface between the microdisk and air. It is obvious that the existence of the hole breaks the original uniform distribution of the light. It can be clearly seen that the light scattering occurs at the position of the hole, and the light emission forms in the direction of 0 deg. The enlarged detail graphs of regions 1, 2, and 3, marked with red rectangles in Fig. 5(a), are shown in Figs. 5(b)–5(d), which are normalized

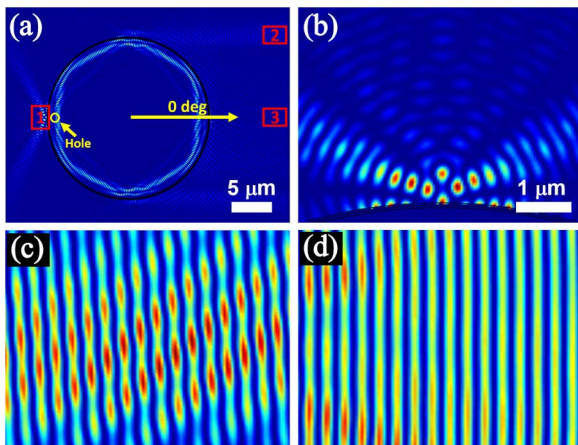


**Fig. 5.** Optical intensity distribution of pierced microdisk based on FDTD simulation. (a) The global intensity distribution. The light scattering occurs at the hole position and the light emission forms in the direction of 0 deg. The definition of the initial angle is the same as Fig. 4(b). (b)–(d) the enlarged detail graphs of regions 1, 2, and 3 in (a).

for showing the light intensity distribution more clearly. Figure 5(b) shows the light scattering at the hole, which is not uniform in direction. The light is in the direction of the disk arc and has a certain angle with the arc. However, it is very weak in perpendicular direction to the disk. The emitting directions of light at regions 2 and 3 are almost 0 deg, shown in Figs. 5(c) and 5(d). Although there are differences in emitting direction, they will be detected simultaneously. This is because the microdisk is very small relative to the light collecting lens, whose focal length is 30 mm. Therefore, because of the existence of the hole, the laser emission is mainly along the direction of 0 deg, which agrees well with the experimental results shown in Fig. 4(b). In addition, in Fig. 4(b), the emitted light intensity in directions of 120 and 240 deg are stronger than the other directions, which can be well explained by the hole scattering shown in Fig. 5(b). Ultimately, the pierced hole located at the edge of the microdisk can provide good characteristics in mode selection and unidirectional emission.

In summary, we accomplished the fabrication of a suspended polymer microdisk with a hole pierced by FsLDW via two-photon polymerization. The pierced microcavity has a high  $Q$  factor and low threshold lasing (compared with the reported polymer microcavity). Because of the existence of the hole, the original regular mode competition is destroyed, which leads to a good single-mode characteristic. Moreover, the emitting laser of the pierced microcavity shows good unidirectional characteristics with the far-field divergence angle about 10 deg. The experimental results have very good consistency with the numerical simulations. The pierced microdisk will play an important role in the field of biological sensing, molecular detection, and integrated photonics.

**Funding.** National Natural Science Foundation of China (NSFC); National Basic Research Program of China (973 program) (91423102, 61590930, 91323301, 2014CB921302, 61435005).

## REFERENCES

1. L. N. He, S. K. Ozdemir, and L. Yang, *Laser Photon. Rev.* **7**, 60 (2013).
2. K. J. Vahala, *Nature* **424**, 839 (2003).
3. T. Grossmann, T. Wienhold, U. Bog, T. Beck, C. Friedmann, H. Kalt, and T. Mappes, *Light: Sci. Appl.* **2**, e82 (2013).
4. J. F. Ku, Q. D. Chen, R. Zhang, and H. B. Sun, *Opt. Lett.* **36**, 2871 (2011).
5. A. B. Matsko, A. A. Savchenkov, D. Strekalov, N. Mohageg, V. S. Ilchenko, and L. Maleki, *Proc. SPIE* **5708**, 242 (2005).
6. P. Michler, A. Kiraz, C. Becher, W. V. Schoenfeld, P. M. Petroff, L. D. Zhang, E. Hu, and A. Imamoglu, *Science* **290**, 2282 (2000).
7. X. D. Fan, I. M. White, S. I. Shopova, H. Y. Zhu, J. D. Suter, and Y. Z. Sun, *Anal. Chim. Acta* **620**, 8 (2008).
8. V. Sandoghdar, F. Treussart, J. Hare, V. Lefèvre-Seguin, J.-M. Raimond, and S. Haroche, *Phys. Rev. A* **54**, R1777 (1996).
9. R. Chen, B. Ling, X. W. Sun, and H. D. Sun, *Adv. Mater.* **23**, 2199 (2011).
10. D. E. Gomez, I. Pastoriza-Santos, and P. Mulvaney, *Small* **1**, 238 (2005).
11. S. Juodkakis, K. Fujiwara, T. Takahashi, S. Matsuo, and H. Misawa, *J. Appl. Phys.* **91**, 916 (2002).
12. V. V. Datsuyk, S. Juodkakis, and H. Misawa, *J. Opt. Soc. Am. B* **22**, 1471 (2005).
13. X. Wu, H. Li, L. Y. Liu, and L. Xu, *Appl. Phys. Lett.* **93**, 081105 (2008).
14. G. D. Chern, H. E. Tureci, A. Douglas Stone, R. K. Chang, M. Kneissl, and N. M. Johnson, *Appl. Phys. Lett.* **83**, 1710 (2003).
15. X. P. Zhan, J. F. Ku, Y. X. Xu, X. L. Zhang, J. Zhao, W. Fang, H. L. Xu, and H. B. Sun, *IEEE Photon. Technol. Lett.* **27**, 311 (2015).
16. J. F. Ku, Q. D. Chen, X. W. Ma, Y. D. Yang, Y. Z. Huang, H. L. Xu, and H. B. Sun, *IEEE Photon. Technol. Lett.* **27**, 1157 (2015).
17. J. Wiersig and M. Hentschel, *Phys. Rev. A* **73**, 031802 (2006).
18. Q. Sun, K. Ueno, H. Yu, A. Kubo, Y. Matsuo, and H. Misawa, *Light: Sci. Appl.* **2**, e118 (2013).
19. M. Malinauskas, A. Zukauskas, S. Hasegawa, Y. Hayasaki, V. Mizeikis, R. Buividas, and S. Juodkakis, *Light: Sci. Appl.* **5**, e16133 (2016).
20. Z. F. Deng, Q. Yang, F. Chen, X. W. Meng, H. Bian, J. L. Yong, C. Shan, and X. Hou, *Opt. Lett.* **40**, 1928 (2015).
21. B. B. Xu, H. Xia, L. G. Niu, Y. L. Zhang, K. Sun, Q. D. Chen, Y. Xu, Z. Q. Lv, Z. H. Li, H. Misawa, and H. B. Sun, *Small* **6**, 1762 (2010).
22. Y. Tian, Y. L. Zhang, J. F. Ku, Y. He, B. B. Xu, Q. D. Chen, H. Xia, and H. B. Sun, *Lab Chip* **10**, 2902 (2010).
23. Y. L. Sun, W. F. Dong, L. G. Niu, T. Jiang, D. X. Liu, L. Zhang, Y. S. Wang, Q. D. Chen, D. P. Kim, and H. B. Sun, *Light: Sci. Appl.* **3**, e129 (2014).
24. T. Grossmann, S. Schleede, M. Hauser, T. Beck, M. Thiel, G. von Freymann, T. Mappes, and H. Kalt, *Opt. Express* **19**, 11451 (2011).
25. J. T. Lin, Y. X. Xu, Z. W. Fang, M. Wang, J. X. Song, N. W. Wang, L. L. Qiao, W. Fang, and Y. Cheng, *Sci. Rep.* **5**, 8072 (2015).
26. J. T. Lin, Y. X. Xu, J. X. Song, B. Zeng, F. He, H. L. Xu, K. Sugioka, W. Fang, and Y. Cheng, *Opt. Lett.* **38**, 1458 (2013).
27. D. Wu, S. Z. Wu, L. G. Niu, Q. D. Chen, R. Wang, J. F. Song, H. H. Fang, and H. B. Sun, *Appl. Phys. Lett.* **97**, 031109 (2010).
28. S. A. Backes, J. R. A. Cleaver, A. P. Heberle, J. J. Baumberg, and K. Kohler, *Appl. Phys. Lett.* **74**, 176 (1999).
29. Q. Song, H. Cao, S. T. Ho, and G. S. Solomon, *Appl. Phys. Lett.* **94**, 061109 (2009).